The CAN-In network: a biologically-inspired model for self-sustained theta oscillations and memory maintenance in the hippocampus

Francesco Giovannini, Beate Knauer, Motoharu Yoshida, Laure Buhry

Title: The CAN-In network: a biologically-inspired model for self-sustained theta oscillations and memory maintenance in the hippocampus
Short Title: The CAN-In model of hippocampal theta oscillations

Francesco Giovannini[1,2,3], Beate Knauer[4,5], Motoharu Yoshida[6], Laure Buhry[2,3*]

[1]Neurosys Team, INRIA CR Nancy Grand Est, Villers-lès-Nancy, F-54600, France
[2]Neurosys Team, CNRS, LORIA UMR 7503, Vandoeuvre-lès-Nancy, F-54500, France
[3]Université de Lorraine, LORIA UMR 7503, Vandoeuvre-lès-Nancy, F-54500, France
[4]Research School, Ruhr University Bochum, 44801 Bochum, Germany
[5]Department of Physiology, Monash University, Clayton, VIC, 3800, Australia
[6]Leibniz Institute for Neurobiology (LIN) and German Center for Neurodegenerative Diseases (DZNE), Magdeburg, 39120, Germany

[*]laure.buhry@inria.fr, Neurosys Team, LORIA, 615 Rue du Jardin Botanique, Vandoeuvre-lès-Nancy, F-54500, France

Submitted to Hippocampus

Keywords: theta oscillations — memory — hippocampus — intrinsic persistent firing

Abbreviations: CAN, Calcium-activated non-specific; PCAN, Pyramidal CAN-equipped neuron; In, Inhibitory interneuron; ACh, Acetylcholine; Cch, Carbachol

Abstract

During working memory tasks, the hippocampus exhibits synchronous theta-band activity, which is thought to be correlated with the short-term memory maintenance of salient stimuli. Recent studies indicate that the hippocampus contains the necessary circuitry allowing it to generate and sustain theta oscillations without the need of extrinsic drive. However, the cellular and network mechanisms supporting synchronous rhythmic activity are far from being fully understood. Based on electrophysiological recordings from hippocampal pyramidal CA1 cells, we present a possible mechanism for the maintenance of such rhythmic theta-band activity in the isolated hippocampus. Our model network, based on the Hodgkin-Huxley formalism, comprising pyramidal neurons equipped with calcium-activated non-specific cationic (CAN) ion channels, is able to generate and maintain synchronized theta oscillations ($4 - 12\,Hz$), following a transient stimulation. The synchronous network activity is maintained by an intrinsic CAN current (I_{CAN}), in the absence of constant external input. The analysis of the dynamics of model networks of pyramidal-CAN and interneurons (CAN-In) reveals that feedback inhibition improves the robustness of fast theta oscillations, by tightening the synchronisation of the pyramidal CAN neurons. The frequency and power of the theta oscillations are both modulated by the intensity of the I_{CAN}, which allows for a wide range of oscillation rates within the theta band. This biologically plausible mechanism for the maintenance of synchronous theta oscillations in the hippocampus aims at extending the traditional models of septum-driven hippocampal rhythmic activity.

Introduction

Working memory is commonly referred to as the ability to retain relevant information for the execution of prospective actions depending on that information [Fuster, 2008]. Although originating from a transient stimulus, the encoded information is thought to be relevant for the task at hand and must therefore be maintained in memory long after the original stimulus has disappeared. Neurophysiological recordings during working memory tasks show increased activation in various brain regions including the hippocampus [Fortin et al., 2002, Sederberg et al., 2007] in the form of synchronous activity at theta-band ($4 - 12\,Hz$) and gamma-band ($\geq 30\,Hz$) frequencies [Buzsáki, 2002, Lisman and Jensen, 2013, Osipova et al., 2006, Nyhus and Curran, 2010]. At the neuronal level, this increased activation happens simultaneously with rapid persistent firing [Fuster and Alexander, 1971], suggesting that this might be a mechanism underlying synchronous oscillations [Lisman, 2010].

Several gamma frequency generators have been identified in the hippocampus (for a comprehensive review see [Bartos et al., 2007]), and these often require local networks of interneurons for precise spike-timing modulation of postsynaptic pyramidal neurons. Conversely, theta oscillations (see [Colgin, 2013] for a review) are thought to be generated extrinsically in the medial septum, and the diagonal band of Broca and entorhinal cortex, which then impose the rhythm on the hippocampal formation via GABAergic and cholinergic projections [Vinogradova, 1995, Tóth et al., 1997, Kocsis et al., 1999, Fischer et al., 1999, Stewart and Fox, 1990]. However, a recent experimental study [Goutagny et al., 2009] has shown that theta oscillations can be generated and maintained intrinsically within the hippocampus, without the need for septal afferents. Therefore, the hippocampus must locally incorporate the necessary cells and circuitry to allow for spontaneous emergence of theta oscillations.

Theoretical studies [White et al., 2000] have hypothesised that, given their slow synaptic kinetics, hippocampal GABAergic oriens lacunosum-moleculare (OLM) neurons [Banks et al., 1998] could account for theta frequency modulation in pyramidal neurons. Intrinsically bursting pyramidal neurons in CA3 [Traub et al., 1989] might also act as theta frequency pacemakers by controlling the rhythm of their postsynaptic targets. However, the hippocampal circuitry involved in both these models requires external stimulation to maintain the oscillations.

Here, we use electrophysiological recordings of persistent firing, pyramidal cells from the CA1 region of the hippocampus as references for our models. Equipped with calcium-activated non-specific cationic (CAN) channels [Partridge and Swandulla, 1988], these neurons are capable of maintaining elevated self-sustained persistent firing for long periods ($> 30\,s$) [Knauer et al., 2013]. The activity is triggered by an initial transient current injection, as short as $200\,ms$, which mimics the stimulus in a delayed match-to-sample working memory task. We demonstrate that glutamatergic synaptic interaction allows a network of hippocampal CAN pyramidal neurons (PCAN) to synchronise their activity in the theta range. These theta oscillations are maintained solely by intrinsic cellular mechanisms, in the absence of external stimulation. The network activity is characterised by three distinct activity patterns: a slow asynchronous regime, a synchronised theta-frequency regime, and a fast gamma regime. Moreover, we show that, adding GABAergic feedback inhibition to these networks enhances theta-band synchronisation. In addition, feedback inhibition provides CAN pyramidal neurons with precise clocking allowing for a wider range of theta frequencies in absence of a long-lasting stimulus.

Our work aims at providing one possible explanation for the generation of theta oscillations in the isolated hippocampus. We hypothesise that local networks of hippocampal persistent firing neurons could provide the neural substrate for theta rhythm generators in the isolated hippocampus.This paper presents one of the first modelling studies showing that theta oscillations can be maintained in CA1, relying solely on intrinsic cellular properties, and without the need for external inputs.

Materials and Methods

Experimental Procedures

All procedures involving animals were in accordance with the guidelines of the animal ethics commission at Ruhr University Bochum. For the physiological recordings from 72 CA1 pyramidal neurons we used 53 Long-Evans rats of either sex (40% males) at an age of 14 - 23 days.

Slice Preparation and Recording Procedures

After the induction of deep general anaesthesia, which was confirmed by the absence of the pinch toe reflex, animals were transcardially perfused with an ice-cold perfusion fluid containing (in mM) 110 CholineCl, 1.25 NaH2PO4, 7 MgCl2, 2.5 KCl, 7 D-Glucose, 3 pyruvic acid, 1 ascorbic acid, 26 NaHCO3, 0.5 CaCl2. The extracted and blocked brain was cut in horizontal slices containing the temporal lobe using a vibratome filled with continuously oxygenated ice-cold perfusion fluid. After at least 1 hr rest in normal ACSF (nACSF) containing (in mM) 124 NaCl, 1.25 NaH2PO4, 1.8 MgSO4, 3 KCl, 10 D-Glucose, 26 NaHCO3, 1.6 CaCl2, slices were individually submerged in the recording chamber containing 34-36C warm oxygenated nACSF that additionally contained ionotropic synaptic transmission blockers (2 mM kynurenic acid and 0.1 mM picrotoxin). Patch pipettes (3-8 M) were filled with an intracellular fluid containing (in mM) 120 K-gluconate, 10 HEPES, 0.2 EGTA, 20 KCl, 2 MgCl2, 7 Phosphocreatine di(tris) salt, 4 Na2ATP, 0.3 GTP, and 0.1% (w/v) biocytin with the pH adjusted to 7.3 using 5 M KOH.

Recordings were obtained with at a sampling rate of 20 kHz with the whole cell patch clamp configuration in the current clamp mode. Recordings were not corrected for a liquid junction potential of 10-13 mV. To assess persistent firing, we stimulated cells with a 2 s long and 100 pA strong square pulse applied to a baseline membrane potential just below their firing threshold. The persistent firing frequency was the average action potential rate during a 3 s interval starting with the stimulus onset. Only presumed CA1 pyramidal neurons without epileptiform activity were analysed. For further details on the equipment and procedures see [Knauer, 2015].

Neuron Model

A single compartment conductance-based model was used to simulate the neurons. The current balance equation of the model, representing the evolution of the cell membrane potential over time, is a modified version of the Hodgkin-Huxley equation [Hodgkin and Huxley, 1952]. The neuron model is based on the one described in [Jochems and Yoshida, 2015].

Pyramidal Cells

The model equation for pyramidal neurons comprises a fast sodium (I_{Na}), potassium (I_K), a leak (I_l) as in [Traub and Miles, 1991], as well as a potassium M-current (I_M) [Yamada et al., 1989] for spike frequency adaptation, a low-threshold calcium current (I_{Ca}) [Reuveni et al., 1993] regulating transmembranal calcium influx, and a CAN current (I_{CAN}) [Destexhe et al., 1994]. Presynaptic spikes received by the neuron generate two synaptic currents I_{synE} and I_{synI} for excitatory and inhibitory synapses respectively. These are summed to produce a total $I_{syn} = I_e + I_i$.

The pyramidal cell model equation takes the form:

$$C_m \cdot \frac{dV_m}{\mathrm{d}t} = -I_l - I_K - I_{Na} - I_M - I_{Ca} - I_{CAN} - I_{syn} + I_{stim} \tag{1}$$

The fast sodium. potassium, and leak current equations are based on the Hodgkin-Huxley model by Traub and Miles [Traub and Miles, 1991], and are defined as:

$$\begin{aligned} I_l &= \overline{g}_l \cdot (V_m - E_l) \\ I_K &= \overline{g}_K \cdot n^4 \cdot (V_m - E_K) \\ I_{Na} &= \overline{g}_{Na} \cdot m^3 \cdot h \cdot (V_m - E_{Na}) \end{aligned}$$

where V_m is the neuron membrane potential, $\overline{g}_x$ is the maximum channel conductance for each current, E_x is the ion channel reversal potential, for $x \in \{ l, K, Na \}$, and h, n, m are the gating variables of the currents which obey the following rule:

$$\frac{\mathrm{d}x}{\mathrm{d}t} = \alpha_x \cdot (1 - x) - (\beta_x \cdot x) \tag{2}$$

for $x \in \{ h, n, m \}$. The α_x and β_x functions are defined below. For the leak, fast sodium and potassium currents:

$$\alpha_m = \frac{0.32 \cdot (13 - V_m + V_T)}{\exp\left(\frac{13 - V_m + V_T}{4}\right) - 1} \qquad \beta_m = \frac{0.28 \cdot (V_m - V_T - 40)}{\exp\left(\frac{V_m - V_T - 40}{5}\right) - 1}$$

$$\alpha_h = 0.128 \cdot \exp\left(\frac{17 - V_m + V_T}{18}\right) \qquad \beta_h = \frac{4}{\exp\left(\frac{40 - V_m + V_T}{5}\right) + 1}$$

$$\alpha_n = \frac{0.032 \cdot (15 - V_m + V_T)}{\exp\left(\frac{15 - V_m + V_T}{5}\right) - 1} \qquad \beta_n = 0.5 \cdot \exp\left(\frac{10 - V_m + V_T}{40}\right)$$

where V_T is a constat used to shift the resting potential of the neuron from the original Hodgkin-Huxley value of $0\,mV$ [Hodgkin and Huxley, 1952] to a more realistic value. In all our simulations $V_T = 55\,mV$.

The M-current implementation is based on [Yamada et al., 1989] and takes the form:

$$I_M = \overline{g}_M \cdot p \cdot (V_m - E_K)$$

where the gating variable p follows the rule defined in Equation 2, and its α and β functions are:

$$\alpha_p = \frac{1}{\tau_M} \cdot \left(3.3 \cdot \frac{\exp\left(\frac{V_m + 35}{20}\right) + \exp\left(-\frac{V_m + 35}{20}\right)}{\exp\left(\frac{-35 - V_m}{10}\right)} + 1 \right)$$

$$\beta_p = \frac{1}{\tau_M} \cdot \left[3.3 \cdot \exp\left(\frac{V_m + 35}{20}\right) + \exp\left(-\frac{V_m + 35}{20}\right) \cdot \left(1 - \frac{1}{\exp\left(\frac{-35 - V_m}{10}\right) + 1} \right) \right]$$

The low-threshold calcium current was modelled like in [Jochems and Yoshida, 2015]:

$$I_{Ca} = \overline{g}_{Ca} \cdot q^2 \cdot r \cdot (V_m - E_{Ca})$$

where the gating variables q and r follow the rule defined in Equation 2, and their α and β functions are:

$$\alpha_q = 0.055 \cdot \frac{-27 - V_m}{\exp\left(\frac{-27 - V_m}{3.8}\right) - 1} \qquad \beta_q = 0.94 \cdot \exp\left(\frac{-75 - V_m}{17}\right)$$

$$\alpha_r = 0.000457 \cdot \exp\left(\frac{-13 - V_m}{50}\right) \qquad \beta_r = 0.0065 \cdot \left[\exp\left(\frac{-15 - V_m}{28}\right) + 1 \right]$$

The transmembranal calcium flux is governed by the calcium current, which causes calcium influx, and a ionic pump, which aims at extruding calcium ions. The calcium dynamics are modelled by the following differential equation [Destexhe et al., 1993]:

$$\frac{\mathrm{d}[\mathrm{Ca}]_{\mathrm{i}}^{2+}}{\mathrm{d}t} = \gamma(I_{Ca}) + \frac{[\mathrm{Ca}]_{\infty}^{2+} - [\mathrm{Ca}]_{\mathrm{i}}^{2+}}{\tau_{CAN}}$$

where $[\mathrm{Ca}]_{\mathrm{i}}^{2+}$ is the intracellular calcium concentration, $\gamma(I_{Ca})$ is a function of I_{Ca} which represents the opening of the calcium channel, $[\mathrm{Ca}]_{\infty}^{2+}$ is a constant representing the calcium concentration when the channel is open for a time interval $\Delta t \to \infty$, and τ_{CAN} is a time constant representing the rate of calcium removal from the cell. The calcium influx is modelled as:

$$\gamma(I_{Ca}) = \begin{cases} \frac{-k_u \cdot I_{Ca}}{area} \cdot \frac{1}{2 \cdot F \cdot depth} & : x \geq 0 \\ 0 & : x < 0 \end{cases}$$

where k_u is a unit conversion constant, $area$ is the surface of the cell membrane, F is Faraday's constant and $depth$ is the depth at which the calcium is stored in the cell.

Part of the intracellular Ca^{2+} ions are in turn responsible for gating calcium-activated non-selective cation (CAN) channels [Partridge et al., 1994]. CAN channels are permeable to K^+ and Na^+ ions [Schultz, 1990] whose flux generates a CAN current I_{CAN}. The CAN current was modelled as in [Destexhe et al., 1994]:

$$I_{CAN} = \overline{g}_{CAN} \cdot s^2 \cdot (V_m - E_{CAN})$$

where the gating variable s follows the rule defined in Equation 2, and its α and β functions are:

$$\begin{aligned} \alpha_s &= \alpha_2([\mathrm{Ca}]_{\mathrm{i}}^{2+}) \cdot T_{adj} \\ \beta_s &= \beta_{CAN} \cdot T_{adj} \\ \alpha_2([\mathrm{Ca_i}]^{2+}) &= \beta_{CAN} \cdot \left(\frac{[\mathrm{Ca}]_{\mathrm{i}}^{2+}}{[\mathrm{Ca}]_{\mathrm{c}}^{2+}} \right)^2 \\ T_{adj} &= 3.0^{\frac{T - 295.15}{10}} \end{aligned}$$

Here, $\alpha_2([\mathrm{Ca}]_{\mathrm{i}}^{2+})$ is a function of the intracellular calcium concentration $[\mathrm{Ca}]_{\mathrm{i}}^{2+}$, β_{CAN} is a constant used to adjust the maximum closing rate of the channel, T_{adj} is a function of the temperature used to adjust the channel opening temperature-dependence, and T is the temperature at which the simulation is run, in Kelvins.

Parameter	Value	Parameter	Value
$\overline{g}_L$	$0.01\,mS\,cm^{-2}$	β_{CAN}	$0.00002\,ms$
E_L	$-70\,mV$	$[\mathrm{Ca}]_{\infty}^{2+}$	$2.4 \cdot 10^{-4}\,mol\,m^{-3}$
$\overline{g}_K$	$5\,mS\,cm^{-2}$	τ_{CAN}	$1000\,ms$
E_K	$-100\,mV$	$[\mathrm{Ca}]_{\mathrm{c}}^{2+}$	$0.75 \cdot 10^{-3}\,mol\,m^{-3}$
$\overline{g}_{Na}$	$50\,mS\,cm^{-2}$	$Temp$	$(36 + 273.15)\,K$
E_{Na}	$50\,mV$	k_u	10^4
$\overline{g}_M$	$0.03\,mS\,cm^2$	$depth$	$1\,\mu m$
τ_M	$1000\,ms$	$area$	$29000\,\mu m^2$
$\overline{g}_{Ca}$	$0.1\,mS\,cm^2$	C_m	$1\,\mu F\,cm^{-2}$
E_{Ca}	$120\,mV$	V_T	$-55\,mV$
$\overline{g}_{CAN}$	$25 \cdot 10^{-3}\,mS\,cm^2$	F	$96489\,C\,mol^{-1}$
E_{CAN}	$-20\,mV$		

Table 1. Pyramidal and CAN neuron parameters.

Inhibitory Cells

Fast-spiking inhibitory cells comprise only the fast sodium (I_{Na}), potassium (I_K), and leak (I_l) currents as in [Kopell et al., 2010]. Hippocampal interneurons were shown in vitro to not display persistent firing in response to a single brief stimulation [Sheffield et al., 2011], and therefore don't require calcium and CAN currents. Fast spiking regimes are obtained by appropriately modifying the parameters of the model equation. The model equations are based on [Kopell et al., 2010]:

$$C_m \cdot \frac{\mathrm{d}V_m}{\mathrm{d}t} = -I_l - I_K - I_{Na} - I_{Syn} \tag{3}$$

where:

$$\begin{aligned} I_l &= \overline{g}_l \cdot (V_m - E_l) \\ I_K &= \overline{g}_K \cdot n^4 \cdot (V_m - E_K) \\ I_{Na} &= \overline{g}_{Na} \cdot m^3 \cdot h \cdot (V_m - E_{Na}) \end{aligned}$$

The activation variables m, h, n obey the following rule:

$$\frac{\mathrm{d}x}{\mathrm{d}t} = \frac{x_\infty - x}{\tau_x} \qquad x_\infty = \frac{\alpha_x}{\alpha_x + \beta_x} \qquad \tau_x = \frac{0.2}{\alpha_x + \beta_x}$$

for $x \in \{ m, h, n \}$. The α and β functions for each activation variable are defined as:

$$\begin{aligned} \alpha_m &= \frac{0.1 \cdot (V_m + 35)}{1 - \exp\left(-\frac{(V_m+35)}{10}\right)} & \beta_m &= 4 \cdot \exp\left(-\frac{(V_m + 60)}{18}\right) \\ \alpha_h &= 0.07 \cdot \exp\left(-\frac{(V_m + 58)}{20}\right) & \beta_h &= \frac{1}{\exp(-0.1 \cdot (V_m + 28)) + 1} \\ \alpha_n &= \frac{0.01 \cdot (V_m + 34)}{1 - \exp(-0.1 \cdot (V_m + 34))} & \beta_n &= 0.125 \cdot \exp\left(-\frac{(V_m + 44)}{80}\right) \end{aligned}$$

Parameter	Value	Parameter	Value
$\overline{g}_l$	$0.1\,mS\,cm^{-2}$	$\overline{g}_{Na}$	$35\,mS\,cm^{-2}$
E_l	$-65\,mV$	E_{Na}	$55\,mV$
$\overline{g}_K$	$9\,mS\,cm^{-2}$	$area$	$14000\,\mu m^2$
E_K	$-90\,mV$	C_m	$1\,\mu F\,cm^{-2}$

Table 2. Inhibitory neuron parameters.

Synaptic Connectivity

The synaptic interactions between the neurons are modelled using appropriate excitatory (I_c) and inhibitory (I_i) synaptic currents. These are governed by mono-exponential differential equations. The synaptic currents were modelled with the following equations:

$$\begin{aligned} I_{syn} &= \sum_{x \in \{ c,i \}} I_x \\ I_x &= g_x \cdot (V_m - E_x) \end{aligned}$$

for $x \in \{ c, i \}$ and $y \in \{ c, i \}$, where E_x is the synaptic resting potential and g_x is the conductance which obeys the following rule, given its time decay constant τ_x:

$$\frac{\mathrm{d}g_x}{\mathrm{d}t} = -\frac{g_x}{\tau_x}$$

Whenever a postsynaptic neuron receives a presynaptic spike its conductance g_x is increased as follows:

$$g_x \leftarrow g_x + w_{yx}$$

where w_{yx} is the connection weight between the presynaptic neuron (identified by y) and the postsynaptic neuron (identified by x). For simplicity we relied on single exponential synapses with an instantaneous channel opening rate. Synaptic weights are normalised according to the network size, to ensure that the average synaptic conductance per neuron remains constant. Unless otherwise specified, the neurons are randomly connected, with a connection probability of 0.4.

Parameter	Value	Parameter	Value
E_c	$0\,mV$	E_i	$-80\,mV$
τ_c	$5\,ms$	τ_i	$10\,ms$

Table 3. Synaptic current parameters.

Network Synchronisation

The network synchronisation is computed using the coherence measure defined in [Wang and Buzsáki, 1996]. The measure computes the pair-wise co-occurrence of neuron action potentials $\kappa_{i,j}(\tau)$ given a time windows of size τ. For any pair of neurons X and Y, given their spike trains represented as a series of ones and zeroes depending on whether the neuron spiked or did not in the time window respectively:

$$X_i(l),\, Y_j(l) \in \{0, 1\}$$
$$l = 1, 2, ..., L \qquad L = \frac{t_{sim}}{\tau} \qquad \tau = 10\,ms$$

where t_{sim} is the duration time of the simulation, and L is the number of time windows of size τ. Increasing the size of τ augments the probability of spike co-occurrence and allowing for larger synchronisation values which might be unrealistic. For all our computations we used $\tau = 10\,ms$, which we deemed small enough to capture the dynamics of the network. The pair-wise coherence measure is quantified as:

$$\kappa_{i,j}(\tau) = \frac{\sum_{l=1}^{L} X_i(l) \cdot Y_j(l)}{\sqrt{\sum_{l=1}^{L} X_i(l) \cdot \sum_{l=1}^{L} Y_j(l)}} \tag{4}$$

The network synchronisation measure is then computed as the average $\kappa_{i,j}(\tau)$ for a randomly sampled subset of neuron pairs in the network.

$$\kappa(\tau) = \frac{\sum_{i,j \in P} \kappa_{i,j}(\tau)}{N} \tag{5}$$

where $P = \{\,(0, 1), (3, 4), ...\,\}$ is a subset of randomly sampled neuron pairs of size N. Unless otherwise specified, the network synchronisation is averaged over a subset containing 10% of the total neuron pairs in the network, without repetitions. $\kappa(\tau)$ is comprised between 0 and 1, representing an asynchronous population firing and fully synchronised firing respectively.

Oscillations

The oscillatory frequencies and power spectra of the neural populations is computed by applying a one-sided Welch transform to the time series of the average membrane potential of the population. This average signal aims at approximating a local field potential recorded with an electrode inserted at the centre of the neuronal population.

Simulations and Data Analysis

The simulations were run using the BRIAN spiking neural network simulator [Goodman and Brette, 2009]. The data analyses and statistical comparisons for both recordings and simulations were performed using Matlab (MathWorks). Average values are represented as mean ± SEM. Statistical significance was a p-value of $\alpha < 0.05$. When comparing the *in vitro* data to 20 simulations p-values were Bonferroni-corrected for multiple comparisons.

Results

In Vitro CAN-Mediated Persistent Firing Frequency

The parameters of the individual cells in the model network are based on *in vitro* recordings of hippocampal CA1 pyramidal cells in the presence of the cholinergic agonist carbachol (Cch). In previous reports [Jochems and Yoshida, 2013, Knauer et al., 2013] we demonstrated that persistent firing in pyramidal neurons of the hippocampus depends on the presence of Cch and is mediated by muscarinic receptor activation. Furthermore, we previously showed that the stimulus duration ($200\,ms$ vs. $2\,s$) does not significantly affect the persistent firing frequency in CA1 pyramidal neurons [Knauer et al., 2013]. Due to a larger sample size and the availability of cells at various Cch concentrations in the $2\,s$ condition compared to the $200\,ms$ condition, we adapted the model parameters to *in vitro* recordings from four separate sets of cells stimulated with a $2\,s$, $100\,pA$ square pulse in the presence of 1, 5, 10, or $20\,\mu M$ Cch ($n = 4, 17, 40, 11$; respectively).

The average persistent firing frequency across all cells *in vitro* was $15.6 \pm 0.6\,Hz$ (Fig. 1 (A), $n = 72$) and did not significantly differ (2-sample T-test with unequal variances, $0.480 \leq p \leq 0.992$) from any of the average persistent firing frequencies of the independent 100 cells in 20 separate simulations of the cells composing the model network ($15.2 \pm 0.27 Hz \leq f \leq 16.0 \pm 0.34\,Hz$). Fig. 1 (C) shows a sample voltage trace recorded from a CA1 pyramidal neuron displaying persistent firing at a frequency of approximately $15\,Hz$ given a $2\,s$ stimulation.

Cholinergic-Dependent Persistent Firing

The presence of 1, 5, 10, or $20\,\mu M$ Cch had a significant effect (one-way ANOVA, $F(3, 68) = 3.02$, $p = 0.036$) on the persistent firing frequency ($9.3 \pm 3.4\,Hz$, $14.7 \pm 1.2\,Hz$, $16.6 \pm 0.8\,Hz$, $15.4 \pm 1.2\,Hz$, respectively) (Fig. 1 (A)). These results indicate that higher Cch concentrations yielded a higher persistent firing frequency. Cholinergic-dependent persistent firing in CA1 pyramidal neurons depends on a calcium-activated non-selective cationic (CAN) current [Jochems and Yoshida, 2015] which is thought to be mediated by canonical transient receptor potential (TRPCs) channels [Reboreda et al., 2011].

Persistent Firing Neuron Model Parameters Extracted from *In Vitro* Recordings

In our model, we adapted Cch concentration levels by varying the strength of the CAN current conductance $\overline{g}_{CAN}$ (Fig.1 (B)). We also introduced Gaussian-distributed heterogeneity in the CAN conductance. Resulting $\overline{g}_{CAN}$ values were grouped into four equidistant intervals of 5, 39, 49, and 7 cells, centred on average $\overline{g}_{CAN}$ values of $38\,\mu S\,cm^{-2}$, $47\,\mu S\,cm^{-2}$, $53\,\mu S\,cm^{-2}$, and $61\,\mu S\,cm^{-2}$, respectively. These groups yielded persistent firing rates of $7.1 \pm 1.6\,Hz$, $14.1 \pm 0.2\,Hz$, $17.5 \pm 0.2\,Hz$, $22.8 \pm 0.6\,Hz$, respectively. We found, in all 20 simulations, that an increase in $\overline{g}_{CAN}$ significantly affected (one-way ANOVA, $F(3, 96) = 176.1$, Bonferroni-corrected $p < 0.001$) the persistent firing frequency of the pyramidal cells composing the model network. Indeed, modifying $\overline{g}_{CAN}$ allowed the model neuron to display a rich array of persistent firing rates. In addition, in accord with the results reported in [Knauer et al., 2013], the stimulus duration has no significant effect on the frequency of

the persistent firing. Fig. 1 (D) shows a sample voltage trace of a model neuron displaying persistent firing at a frequency of approximately $15\,Hz$ given a $2\,s$ stimulation.

The Pyramidal CAN Network Shows a Rich Array of Firing Regimes

Having obtained a biologically-inspired model of CA1 persistent firing pyramidal neurons (PCAN), we turned our attention to the dynamics of a population comprising 100 of such interconnected neurons. The population was stimulated with a strong transient current injection $I_{stim} = 200\,pA$ lasting $\Delta t = 250\,ms$, which would cause an individual, unconnected, PCAN neuron to display persistent firing at an average rate of $f = 16.00 \pm 0.26\,Hz$. The transient stimulus emulates the brief cue presentation in a delayed match-to-sample working memory task. For this purpose we chose the shortest possible duration which would elicit persistent firing in most neurons, in accord with the experimental data.

Similarly as in [Jochems and Yoshida, 2015], we found that the CAN current allows the PCAN network to display a wide range of firing rates as the weights of the excitatory synapses are increased (Fig. 2 (F)), by acting on the w_{cc} parameter. In the absence of CAN current ($\overline{g}_{CAN} = 0\,S\,cm^{-2}$), the population remained mostly quiescent ($f = 0\,Hz$) after the stimulus (Fig. 2 (D)), for connection weight values of $0 \leq w_{cc} \leq 1.08\,nS$. Strengthening the synaptic connections ($1.08\,nS < w_{cc} \leq 1.32\,nS$) accelerated the population frequency, as the increased excitation allowed the network activity to persist for a few milliseconds ($0.08\,Hz \leq f \leq 3.56\,Hz$) after the stimulation was removed, without producing long-lasting persistent firing (Fig. 2 (E)). When the synaptic strength was increased above $1.32\,nS$, the population abruptly displayed fast persistent firing with frequency values greater than $120\,Hz$ (Fig. 2 (C)). In contrast, our CAN-equipped population was able to generate a continuous range of persistent firing frequencies comprised between $14\,Hz$ and $200\,Hz$, given increasing pyramidal-to-pyramidal connection strengths. Furthermore, the CAN network displayed three different population firing regimes: a slow regime with firing rates $14\,Hz \leq f \leq 21\,Hz$ (Fig. 2 (A)), a synchronous bursting regime (Fig. 2 (B)), and a fast regime with firing rates $f \geq 117\,Hz$ (Fig. 2 (C)).

The transition between asynchronous slow regime and synchronous bursting depended on the interaction between increased synaptic excitation and the spike-frequency adaptation provided by the M current. A careful balance between these two currents allowed synchronous oscillations at frequencies within the theta-band [Colgin, 2013] to emerge (Fig. 3 (A) shows a sample raster plot with synchronous activity at $f_{osc} = 5.46\,Hz$ with a synchronisation of $\kappa(\tau) = 0.38$. Increasing synaptic strengths over a certain threshold, merged the bursts into fast gamma population activity, as the local excitation prevailed over the adaptation. Weakening or disabling the M current, by acting on its conductance $\overline{g}_M$, caused the bursting regime to disappear in favour of an asynchronous firing regime whose frequency increased as PCAN-to-PCAN synapses were strengthened. Conversely, gradually strengthening the M current ($\overline{g}_M \geq 12\,nS$) slowed the oscillatory frequency and produced thinner bursts which eventually degraded into singlet spikes.

These results are independent of network size and connection probability.

Synchronisation in a Pyramidal CAN and Interneuron (CAN-In) Network

We then connected the CAN pyramidal network to a population of inhibitory neurons (In) in an attempt to synchronise the network activity by leveraging a PING-like [Kopell et al., 2010] mechanism. The population of fast-spiking interneurons was driven solely by excitatory input from PCAN neurons, and in turn provided them with strong slow-inactivating feedback inhibition. Our results show that such feedback inhibition enhanced the synchrony of CAN-mediated oscillatory activity (Fig. 4 (E)). Given a wide range of PCAN-to-PCAN connection strengths, stronger feedback inhibition always led to an increase in network activity synchronisation. Strengthening inhibitory to CAN connections in a CAN-Inh network displaying asynchronous persistent firing (Fig. 4 (A), $\kappa(\tau) = 0.32$ with $w_{ic} = 0\,nS$) slowly synchronises the activity in tight narrow bands (Fig. 4 (D), $\kappa(\tau) \geq 0.66$ with $w_{ic} \geq 0\,0.8nS$. However, if in the absence of inhibition the network displays synchronous bursts of activity (Fig. 3 (B),

$\kappa(\tau) = 0.66$ with $w_{ic} = 0\,nS$), increasing the inhibitory feedback will first cause a desynchronisation as the bursts are decoupled (Fig. 4 (C), $0.48 \leq \kappa(\tau) \leq 0.59$ with $0.4\,nS \leq w_{ic} \leq 0.7\,nS$), until these become narrow bands of synchronous doublets or singlets and the overall network synchronisation increases (Fig. 4 (D), $0.66 \leq \kappa(\tau) \leq 0.77$ with $0.8\,nS \leq w_{ic} \leq 2\,nS$).

Similarly as in a PING [Kopell et al., 2010] setting, feedback inhibition provides pyramidal neurons with precise windows of increased excitability in which they are synchronously activated. A sample raster plot is shown in Fig. 3 (B). The activity exhibited by our CAN-In network was more tightly synchronised ($\kappa(\tau) = 0.78$), compared with that displayed by the network of solely pyramidal CAN neurons ($\kappa(\tau) = 0.38$). The fastest-attainable oscillatory frequency in the CAN-In network was $f_{osc} = 11\,Hz$, and depended on the maximum firing rate of the CAN-mediated persistent activity, and therefore on the CAN conductance. Increasing feedback inhibition strength above a certain threshold caused it to annihilate the effect of local PCAN-PCAN excitation, and the network activity reverted to an asynchronous firing regime driven solely by the CAN current.

To verify that the synchronous activity was maintained by CAN-persistent firing, we removed the CAN current from the pyramidal population in the CAN-In network. Solely the pyramidal neurons were injected with the same strong transient stimulus as in all our simulations. In the absence of CAN current, and with weak local excitation ($w_{cc} \leq 0.90\,nS$), the pyramidal network activity stopped after the external stimulus disappeared. However, in the presence of strong pyramidal-to-pyramidal excitatory connections ($w_{cc} \geq 1.36\,nS$), the pyramidal population displayed fast ($f \geq 100\,Hz$) persistent firing activity (similar to the one displayed in Fig. 2 (C)) maintained by the recurrent synaptic connections alone. Simulating the effects of feedback inhibition on this activity yielded monostable dynamics in which the persistent activity either swamped the network, as the inhibition failed to control the strength of the excitation, or faded away, as the inhibition prevailed over the excitation. Careful fine-tuning of excitatory and inhibitory connection weights could allow for richer dynamics [Compte, 2006, Wang, 2001], although this remains outside the scope of our current work.

Theta Oscillations Are Modulated by CAN Conductance

The CAN current conductance modulated theta oscillations, which accelerated or decelerated proportionally to changes in values of $\overline{g}_{CAN}$, within a certain parameter range. Increasing the CAN conductance produced faster oscillations, with frequencies ranging between $4\,Hz$ and $11\,Hz$. In addition, the computed theta-band power spectrum (Fig. 5 (A)) of the network activity reflected an increase in power in the theta band, as well as accelerated frequencies, as CAN conductance is increased. The oscillatory frequencies of the PCAN population varied between $4\,Hz \leq f_{osc} \leq 7\,Hz$ for $\mathcal{N}(33,5)\,\mu S\,cm^{-2} \leq \overline{g}_{CAN} \leq \mathcal{N}(55,5)\,\mu S\,cm^{-2}$, $\overline{g}_M = 90\,\mu S\,cm^{-2}$, and $w_{cc} = 0.51\,nS$. The maximum theta power was at $f_{osc} = 4.88\,Hz$ for $\overline{g}_{CAN} = \mathcal{N}(46.5,5)\,\mu S\,cm^{-2}$.

Feedback inhibition also affected theta oscillation frequencies by accelerating them as inhibitory-to-PCAN pyramidal synapses were strengthened. Our results indicate that, in the case of the CAN-In network, the strength of the CAN current modulated both theta power and oscillation frequencies (Fig. 5 (B)). Here, the average oscillation rate of the CAN pyramidal population was $f_{osc} = 7.16 \pm 2.66\,Hz$. The oscillatory frequencies of the isolated PCAN population varied between $4\,Hz \leq f_{osc} \leq 11\,Hz$ for $\mathcal{N}(28,5)\,\mu S\,cm^{-2} \leq \overline{g}_{CAN} \leq \mathcal{N}(64,5)\,\mu S\,cm^{-2}$, $\overline{g}_M = 90\,\mu S\,cm^{-2}$, and $w_{cc} = 1.4\,nS$. Furthermore, the power spectrum of the CAN Pyramidal neurons firing activity showed a peak at $f_{osc} = 8.54\,Hz$ for $\overline{g}_{CAN} = \mathcal{N}(56.9,5)\,\mu S\,cm^{-2}$.

The Synchronous Firing Regime Resembles Gamma-in-Theta Rhythms

The oscillatory frequencies displayed by the CAN population, both with and without inhibition, closely resemble those of nested gamma in theta rhythms as illustrated in Fig. 3 (C). As previously described, the neurons synchronise their activity in theta-frequency bursts of activity ($f_{osc} = 5.46\,Hz$

in Fig. 3 (A)). Investigating the firing patterns of the synchronous bursting regime (Fig. 3 (A)) yielded a synchronisation of $\kappa(\tau) = 0.38$, which was higher than that displayed by the slow firing regime (Fig. 2 (A)) at $\kappa(\tau) = 0.24$. In addition, the intra-burst frequencies were within the gamma band ($f_{intra} = 38.03 \pm 0.61\,Hz$).

Feedback inhibition (Fig. 3 (B)) further tightened the synchronisation of intra-burst spikes, increasing the coherence value to $\kappa(\tau) = 0.78$. As a result, the oscillatory frequency of the PCAN network accelerated to $f_{osc} = 6.91\,Hz$. In this configuration, the CAN population fires synchronously with an average robust intra-burst frequency of $f_{intra} = 57.29 \pm 1.35\,Hz$.

Discussion

CAN-Mediated Synchronous Oscillations

In this paper we present a biologically-inspired model of self-sustained hippocampal oscillations which relies on intrinsic cellular properties commonly found in hippocampal pyramidal neurons [Knauer et al., 2013, Jochems and Yoshida, 2013]. We fitted our model parameters to experimental recordings from CA1 persistent firing cells. The behaviour of our cell model is in very good accordance with the biological data (Fig. 1). Our results demonstrate that synchronous rhythmic activity can be maintained in a network of CAN-equipped persistent firing pyramidal neurons, in the absence of external stimulation. The CAN-mediated rhythm generator relies upon the interaction between local excitation provided by synaptic activity, and the hyperpolarisation provided by a modulating potassic M current. At each firing cycle, the persistent firing activity mediated by the CAN current increases postsynaptic excitation within the network. As a result, every action potential strengthens the M current which eventually temporarily interrupts the network activity by terminating the spiking burst. The frequency of the persistent firing acts as a pacemaker, precisely regulating the onset of the oscillatory activity.

This mechanism is similar to that described in [Aoyagi et al., 2003], in which a CAN-like current provides depolarising after potentials (DAPs) which, when carefully balanced with after hyperpolarising potentials (AHPs), allows single neurons to fire bursts of two or more spikes. In our work and in that of Aoyagi and colleagues [Aoyagi et al., 2003], the pyramidal neurons are intrinsically rhythmical, although not intrinsically bursting (See Fig. S2 (A) and (B) for sample voltage traces). This rhythm can be entrained in their postsynaptic targets in the form of rapid bursts. In our model the bursts of activity persist over long time spans and are maintained without the need for external stimulation, in contrast with the bursting neuron model [Aoyagi et al., 2003] which requires constant stimulation. This allows our network of CAN pyramidal neurons to simulate the hippocampal firing regimes commonly recorded throughout the delay phase of delayed memory tasks [Fransén et al., 2002], during which the hippocampus displays elevated firing, initiated by a transient stimulus salient enough to be retained long after it ceased. Our results demonstrate that the network elicits an ample range of biologically plausible firing rates which are supported solely by the CAN current, suggesting that the CAN current could contribute to the stability and robustness of rhythmic activity of local populations of hippocampal pyramidal neurons.

Recent studies have identified CAN-mediated persistent firing in CA1 [Knauer et al., 2013], an area which is commonly believed to comprise significantly less recurrent connectivity than other hippocampal regions [Deuchars and Thomson, 1996]. These results are in accord with those presented here, in that our network model relies upon a relatively sparse connectivity.

Moreover, the density of the connections within the network do not significantly affect the population firing regimes, and strong recurrent connections alone do not yield biologically realistic firing frequencies (Fig. 2 (F)). Network firing rates and oscillation frequencies are maintained solely by the intensity of the CAN current. Taken together, these observations suggest that our model could be used to represent several different hippocampal areas.

Theta Oscillations in the Isolated Hippocampus

A vast body of literature has highlighted the importance of the medial septum in the generation and maintenance of theta-frequency hippocampal oscillations [Vinogradova, 1995, Tóth et al., 1997, Kocsis et al., 1999, Fischer et al., 1999, Stewart and Fox, 1990]. Nevertheless, the results from a recent study [Goutagny et al., 2009] supported by existing theoretical models [White et al., 2000, Traub et al., 1989] indicate that the hippocampus might possess the necessary circuitry to sustain theta oscillations in the absence of septal drive. Therefore, intrinsic mechanisms within the hippocampus might be required to support theta oscillations triggered by projections from the the medial septum.

Here, we present a simple hippocampal network comprising at most two types of cell. The crucial feature of our model is that local networks of CAN-equipped pyramidal neurons, independent of extrinsic septal drive, can contribute to maintaining theta rhythms within the hippocampus. Therefore, we hypothesise that local circuits comprising CAN pyramidal neurons could provide the neural basis for hippocampal theta oscillations.

Theta frequency and power are both modulated by the intensity of the intrinsic CAN current, which allows for a rich range of oscillation frequencies within the theta band ($4 - 12\,Hz$). CAN channels are modulated by muscarinic acetylcholine receptors [Magistretti et al., 2004] which could be the target of cholinergic projections, providing a stimulation triggering and modulating hippocampal theta oscillations. In the absence of septal afferents, the activation of the CAN current in the pyramidal neurons may originate from local populations of cholinergic interneurons [Frotscher et al., 1986, Yi et al., 2015]. The cholinergic activation could also derive from cholinergic interneurons in the medial septum [Simon et al., 2006], which do not display rhythmic theta firing patterns and are thus thought to act solely as frequency modulators for hippocampal theta oscillators [Colgin, 2013].

Existing models [White et al., 2000] of hippocampal theta require the presence of slow-inactivating inhibition mediated by oriens lacunosum-moleculare (OLM) interneurons, forming a tightly coupled oscillator with their postsynaptic pyramidal neurons [Cobb et al., 1995]. The OLM neurons provide the pyramidal neurons with precise windows of enhanced excitability, synchronising their activity at theta-band frequencies. This circuitry seems to play an important role in the maintenance of theta oscillations in the isolated hippocampus [Goutagny et al., 2009], although the provenance of the inhibitory afferents involved in the circuit remains unclear. In our model, a single type of CAN pyramidal cell is necessary and sufficient for the appearance of theta oscillations, due to its inherent rhythmicity and spike-frequency adaptation. Therefore, our work could provide a simpler explanation for this phenomenon. Including feedback inhibition to these pyramidal neurons merely enhances the synchronisation of the CAN population. Moreover, inhibition improves the robustness of fast theta oscillations by precisely modulating the inter-burst interval of the pyramidal population.

Implications for Hippocampal Theta

Although the septum has been demonstrated to be necessary for the generation of hippocampal theta oscillation, the hippocampus is also thought to rely on its intrinsic properties to maintain this synchronous activity which is crucial to perform working memory tasks. Taken together, our results show that maintenance of rhythmic activity within the hippocampus in the absence of extrinsic drive can be achieved by leveraging intrinsic cellular mechanisms, namely CAN-mediated persistent firing.

As a conclusion, our model possesses various essential features supporting the maintenance of theta oscillations in the isolated hippocampus.

Acknowledgements

We thank the CNRS for funding the Mnemanes project (PEPS JCJC) led by Laure Buhry. We thank Ulf Eysel and Denise Manahan-Vaughan for providing the *in vitro* recording set-up. The contribution

of Beate Knauer was funded by a PhD fellowship of the International Graduate School of Neuroscience at the Ruhr University Bochum, and a Gateway Fellowship of the Ruhr University Research School PLUS, funded by Germany's Excellence Initiative [DFG GSC 98/3]. The authors declare no conflict of interest.

References

[Aoyagi et al., 2003] Aoyagi, T., Takekawa, T., and Fukai, T. (2003). Gamma rhythmic bursts: coherence control in networks of cortical pyramidal neurons. *Neural computation*, 15(5):1035–61.

[Banks et al., 1998] Banks, M. I., Li, T.-B., and Pearce, R. A. (1998). The Synaptic Basis of GABAA,slow. *The journal of neuroscience*, 18(4):1305–1317.

[Bartos et al., 2007] Bartos, M., Vida, I., and Jonas, P. (2007). Synaptic mechanisms of synchronized gamma oscillations in inhibitory interneuron networks. *Nature reviews. Neuroscience*, 8(January):45–56.

[Buzsáki, 2002] Buzsáki, G. (2002). Theta Oscillations in the Hippocampus. *Neuron*, 33(f):325–340.

[Cobb et al., 1995] Cobb, S. R., Buhl, E. H., Halasy, K., Paulsen, O., and Somogyi, P. (1995). Synchronization of neuronal activity in hippocampus by indivicual GABAergic interneurons. *Nature*, 378(6552):75–8.

[Colgin, 2013] Colgin, L. L. (2013). Mechanisms and functions of theta rhythms. *Annual review of neuroscience*, 36:295–312.

[Compte, 2006] Compte, A. (2006). Computational and in vitro studies of persistent activity: edging towards cellular and synaptic mechanisms of working memory. *Neuroscience*, 139(1):135–51.

[Destexhe et al., 1993] Destexhe, A., Babloyantz, A., and Sejnowski, T. J. (1993). Ionic mechanisms for intrinsic slow oscillations in thalamic relay neurons. *Biophysical journal*, 65(4):1538–52.

[Destexhe et al., 1994] Destexhe, A., Contreras, D., Sejnowski, T. J., and Steriade, M. (1994). A model of spindle rhythmicity in the isolated thalamic reticular nucleus. *Journal of neurophysiology*, 72(2):803–18.

[Deuchars and Thomson, 1996] Deuchars, J. and Thomson, A. M. (1996). CA1 pyramid-pyramid connections in rat hippocampus in vitro: Dual intracellular recordings with biocytin filling. *Neuroscience*, 74(4):1009–1018.

[Fischer et al., 1999] Fischer, Y., Gaehwiler, B. H., and Thompson, S. M. (1999). Activation of intrinsic hippocampal theta oscillations by acetylcholine in rat septo-hippocampal cocultures. *The Journal of Physiology*, 519(2):405–413.

[Fortin et al., 2002] Fortin, N. J., Agster, K. L., and Eichenbaum, H. B. (2002). Critical role of the hippocampus in memory for sequences of events. *Nature neuroscience*, 5(5):458–62.

[Fransén et al., 2002] Fransén, E., Alonso, A., and Hasselmo, M. E. (2002). Simulations of the Role of the Muscarinic-Activated Calcium- Sensitive Nonspecific Cation Current I NCM in Entorhinal Neuronal. *The Journal of neuroscience : the official journal of the Society for Neuroscience*, 22(3):1081–1097.

[Frotscher et al., 1986] Frotscher, M., Schlander, M., and Leranth, C. (1986). Cholinergic neurons in the hippocampus. *Cell and Tissue Research*, 246:293–301.

[Fuster, 2008] Fuster, J. (2008). Executive Function. In *The Prefrontal Cortex*, chapter Human Neur, pages 171–219. Academic Press, 4 edition.

[Fuster and Alexander, 1971] Fuster, J. and Alexander, G. E. (1971). Neuron Activity Related to Short-Term Memory. *Science*, 173(3997):652–654.

[Goodman and Brette, 2009] Goodman, D. F. M. and Brette, R. (2009). The Brian simulator. *Frontiers in Neuroscience*, 3(SEP):192–197.

[Goutagny et al., 2009] Goutagny, R., Jackson, J., and Williams, S. (2009). Self-generated theta oscillations in the hippocampus. *Nature neuroscience*, 12(12):1491–3.

[Hodgkin and Huxley, 1952] Hodgkin, A. L. and Huxley, A. (1952). A Quantitative Description of Membrane Current and Application to Conduction and Excitation in Nerve. *Journal of Physiology*, 117:500–544.

[Jochems and Yoshida, 2013] Jochems, A. and Yoshida, M. (2013). Persistent firing supported by an intrinsic cellular mechanism in hippocampal CA3 pyramidal cells. *The European journal of neuroscience*, 38(2):2250–9.

[Jochems and Yoshida, 2015] Jochems, A. and Yoshida, M. (2015). A robust in vivo-like persistent firing supported by a hybrid of intracellular and synaptic mechanisms. *PloS one*, 10(4):e0123799.

[Knauer, 2015] Knauer, B. (2015). *Persistent firing and depolarization block in rat Ca1 pyramidal neurons*. PhD thesis, Ruhr University Bochum.

[Knauer et al., 2013] Knauer, B., Jochems, A., Valero-Aracama, M. J., and Yoshida, M. (2013). Long-lasting intrinsic persistent firing in rat CA1 pyramidal cells: a possible mechanism for active maintenance of memory. *Hippocampus*, 23(9):820–31.

[Kocsis et al., 1999] Kocsis, B., Bragin, a., and Buzsáki, G. (1999). Interdependence of multiple theta generators in the hippocampus: a partial coherence analysis. *The Journal of neuroscience : the official journal of the Society for Neuroscience*, 19(14):6200–6212.

[Kopell et al., 2010] Kopell, N. J., Boergers, C., Pervouchine, D., Malerba, P., and Tort, A. (2010). Gamma and theta rhythms in biophysical models of hippocampal circuits. In Cutsuridis, V., Graham, B., Cobb, S., and Vida, I., editors, *Hippocampal Microcircuits A Computational Modeler's Resource Book*, chapter Gamma and, pages 423–457. Springer New York, New York, NY.

[Lisman, 2010] Lisman, J. (2010). Working memory: The importance of theta and gamma oscillations. *Current Biology*, 20(11):R490–R492.

[Lisman and Jensen, 2013] Lisman, J. E. and Jensen, O. (2013). The Theta-Gamma Neural Code. *Neuron*, 77(6):1002–1016.

[Magistretti et al., 2004] Magistretti, J., Ma, L., Shalinsky, M. H., Lin, W., Klink, R., and Alonso, A. (2004). Spike Patterning by Ca2+-Dependent Regulation of a Muscarinic Cation Current in Entorhinal Cortex Layer II Neurons. *Journal of Neurophysiology*, 92:1644–1657.

[Nyhus and Curran, 2010] Nyhus, E. and Curran, T. (2010). Functional role of gamma and theta oscillations in episodic memory. *Neuroscience and biobehavioral reviews*, 34(7):1023–35.

[Osipova et al., 2006] Osipova, D., Takashima, A., Oostenveld, R., Fernández, G., Maris, E., and Jensen, O. (2006). Theta and gamma oscillations predict encoding and retrieval of declarative memory. *The Journal of neuroscience : the official journal of the Society for Neuroscience*, 26(28):7523–31.

[Partridge et al., 1994] Partridge, L. D., Muller, T. H., and Swandulla, D. (1994). Non-selective channels in the nervous system. *Brain research reviews*, 19:319–325.

[Partridge and Swandulla, 1988] Partridge, L. D. and Swandulla, D. (1988). Calcium-activated non-specific cation channels. *Trends in neurosciences*, 11(2):69–72.

[Reboreda et al., 2011] Reboreda, A., Jiménez-Dìaz, L., and Navarro-López, J. D. (2011). TRP Channels and Neural Persistent Activity. In Islam, M. S., editor, *Transient Receptor Potential Channels*, volume 704, chapter 32, pages 517–530. Springer Netherlands, 1 edition.

[Reuveni et al., 1993] Reuveni, I., Friedman, A., Amitai, Y., and Gutnick, M. J. (1993). Stepwise repolarization from Ca2+ plateaus in neocortical pyramidal cells: evidence for nonhomogeneous distribution of HVA Ca2+ channels in dendrites. *The Journal of neuroscience : the official journal of the Society for Neuroscience*, 13(11):4609–21.

[Schultz, 1990] Schultz, J. E. (1990). Potassium Channels. Structure, classification, function and therapeutic potential. Hrsg. Nigel S. Cook. Allis Horwood, Chichester, UK. 1990. 412 S., zahlr. Abb., geb., $ 59.95. *Pharmazie in Unserer Zeit*, 19(4):172–172.

[Sederberg et al., 2007] Sederberg, P. B., Schulze-Bonhage, A., Madsen, J. R., Bromfield, E. B., Litt, B., Brandt, A., and Kahana, M. J. (2007). Gamma oscillations distinguish true from false memories. *Psychological science : a journal of the American Psychological Society / APS*, 18:927–932.

[Sheffield et al., 2011] Sheffield, M. E. J., Best, T. K., Mensh, B. D., Kath, W. L., and Spruston, N. (2011). Slow integration leads to persistent action potential firing in distal axons of coupled interneurons. *Nature neuroscience*, 14(2):200–207.

[Simon et al., 2006] Simon, A. P., Poindessous-Jazat, F., Dutar, P., Epelbaum, J., and Bassant, M.-H. (2006). Firing Properties of Anatomically Identified Neurons in the Medial Septum of Anesthetized and Unanesthetized Restrained Rats. *The Journal of Neuroscience*, 26(35):9038–9046.

[Stewart and Fox, 1990] Stewart, M. and Fox, S. E. (1990). Do septal neurons pace the hippocampal theta rhythm? *Trends in Neurosciences*, 13(5):163–169.

[Tóth et al., 1997] Tóth, K., Freund, T. F., and Miles, R. (1997). Disinhibition of rat hippocampal pyramidal cells by GABAergic afferents from the septum. *The Journal of Physiology*, 500 (Pt 2:463–74.

[Traub and Miles, 1991] Traub, R. D. and Miles, R. (1991). *Neuronal Networks of the Hippocampus*. Cambridge University Press, New York.

[Traub et al., 1989] Traub, R. D., Miles, R., and Wong, R. K. S. (1989). Model of the origin of rhythmic population oscillations in the hippocampal slice. *Science*, 243:1319–1325.

[Vinogradova, 1995] Vinogradova, O. S. (1995). Expression, control, and probable functional significance of the neuronal theta-rhythm. *Progress in Neurobiology*, 45(6):523–583.

[Wang, 2001] Wang, X.-J. (2001). Synaptic reverberation underlying mnemonic persistent activity. *Trends in neurosciences*, 24(8):455–63.

[Wang and Buzsáki, 1996] Wang, X.-J. and Buzsáki, G. (1996). Gamma oscillation by synaptic inhibition in a hippocampal interneuronal network model. *The Journal of Neuroscience : the official journal of the Society for Neuroscience*, 16(20):6402–13.

[White et al., 2000] White, J. A., Banks, M. I., Pearce, R. A., and Kopell, N. J. (2000). Networks of interneurons with fast and slow gamma-aminobutyric acid type A (GABAA) kinetics provide substrate for mixed gamma-theta rhythm. *Proceedings of the National Academy of Sciences of the United States of America*, 97(14):8128–33.

[Yamada et al., 1989] Yamada, W. M., Koch, C., and Adams, P. R. (1989). Multiple Channels and Calcium Dynamics. In Koch, C. and Segev, I., editors, *Methods in neuronal modeling*, pages 97–134. MIT Press.

[Yi et al., 2015] Yi, F., Catudio-Garrett, E., G??briel, R., Wilhelm, M., Erdelyi, F., Szabo, G., Deisseroth, K., and Lawrence, J. (2015). Hippocampal "cholinergic interneurons" visualized with the choline acetyltransferase promoter: Anatomical distribution, intrinsic membrane properties, neurochemical characteristics, and capacity for cholinergic modulation. *Frontiers in Synaptic Neuroscience*, 7(MAR):1–18.

Figure Legends

Fig. 1. The activation of CAN receptors modulates the persistent firing frequency of hippocampal neurons, both *in vitro* and in the model. (A) The carbachol concentration (μM) modulates the persistent firing frequency recorded *in vitro*. (B) Similary, the CAN conductance (g_{CAN}) modulates the persistent firing frequency of the simulated neurons. Line and asterisks over bars indicate statistical significance. Numbers inside the bars represent the cell count. (C) Sample *in-vitro* recording of the membrane potential (V_m) of one CA1 pyramidal neuron showing approximately $6\,Hz$ persistent firing after a $2\,s$ stimulation. (D) Sample voltage trace for one simulated neuron showing approximately $6\,Hz$ persistent firing after a $2\,s$ stimulation. In the voltage trace plots the bottom line represents the applied square pulse stimulation current. Persistent firing is elicited after a brief ($2\,s$) stimulation. Parameters for the CAN pyramidal neurons shown in the histogram are: $g_{\text{CAN}} = \mathcal{N}(50, 5)\,\mu S\,cm^{-2}$, $g_{\text{M}} = 90\,\mu S\,cm^{-2}$.

Fig. 2. The CAN current activation allows a 100-cell network to display persistent firing in biologically plausible frequency bands. (A) CAN-enabled Network – Sample raster plot of the slow regime ($0\,nS \leq w_{cc} \leq 0.45\,nS$), with a population firing rate of $f = 19.45\,Hz$ for $w_{cc} = 0.36\,nS$. (B) CAN-enabled Network – Sample raster plot of the synchronous bursting firing regime ($0.48\,nS \leq w_{cc} \leq 1.17\,nS$), showing $f_{osc} = 5\,Hz$ oscillations for $w_{cc} = 0.72\,nS$. (C) CAN-enabled Network – Sample raster plot of the fast firing regime ($w_{cc} \geq 1.2\,nS$), with a population firing rate $f = 117.3\,Hz$ for $w_{cc} = 1.2\,nS$. (D) CAN-disabled Network – Sample raster plot showing the lack of persistent firing in the absence of CAN current ($0\,nS \leq w_{cc} \leq 1.08\,nS$). ($E$) CAN-disabled Network – Sample raster plot showing firing activity persisting for a few milliseconds after the stimulation is removed ($1.11\,nS \leq w_{cc} \leq 1.32\,nS$), with a population firing rate $0.08\,Hz \leq f \leq 3.56\,Hz$. ($F$) The population firing frequencies of the CAN pyramidal network span $14\,Hz \leq f \leq 120\,Hz$, with $0\,nS \leq w_{cc} \leq 1.23\,nS$. The CAN network (top line) displays three different firing regimes: a slow regime with firing rates $14\,Hz \leq f \leq 21\,Hz$ (A), a synchronous bursting regime (B), and a fast spiking regime with firing rates $f \geq 117\,Hz$ (C). Conversely, a pyramidal network without CAN current (bottom line) does not display such a rich array of firing regimes (D and E). Parameters are: $g_{\text{CAN}} = \mathcal{N}(50, 5)\,\mu S\,cm^{-2}$, $g_{\text{M}} = 90\,\mu S\,cm^{-2}$, $0 \leq w_{cc} \leq 1.5\,nS$.

Fig. 3. Comparison of CAN and CAN-In network dynamics. (A) Raster plot for the 100-cell CAN pyramidal network, showing $5.46\,Hz$ oscillations with a synchronisation of $\kappa(\tau) = 0.38$, $\tau = 10\,ms$. (B) Raster plot for the CAN-Inhibitory network comprising 75 CAN pyramidal cells (cell number $0 - 74$, blue diamonds) and 25 inhibitory cells (cell number $75 - 99$, black dots), showing $6.91\,Hz$ oscillations with a synchronisation of $\kappa(\tau) = 0.78$, $\tau = 10\,ms$. In both plots the red line below the raster represents the applied stimulation current. (C) LFP signal computed from the spiking activity of the CAN pyramidal network shows nested gamma in theta oscillations. (D) LFP signal computed from the spiking activity of the CAN-Inhibitory network shows nested gamma in theta oscillations with higher amplitudes compared to the CAN pyramidal network. Parameters for the CAN-only network are: $g_{\text{CAN}} = \mathcal{N}(50, 5)\,\mu S\,cm^{-2}$, $g_{\text{M}} = 90\,\mu S\,cm^{-2}$, $w_{cc} = 0.48\,nS$. Parameters for the CAN-Inhibitory network are: $g_{\text{CAN}} = \mathcal{N}(50, 5)\,\mu S\,cm^{-2}$, $g_{\text{M}} = 90\,\mu S\,cm^{-2}$, $w_{cc} = 1.44\,nS$, $w_{ci} = 1\,nS$, $w_{ii} = 1.0\,nS$, $w_{ic} = 1.2\,nS$.

Fig. 4. Feedback inhibition synchronises CAN-mediated persistent activity. (A) Sample raster plot of the asynchronous firing regime showing a synchrony measure of $\kappa(\tau) = 0.32$ in the absence of inhibitory feedback ($w_{ic} = 0\,nS$) and weaker local excitation ($w_{cc} < 0.8\,nS$). (B) Sample raster plot of the synchronous bursting firing regime showing a synchrony measure of $\kappa(\tau) = 0.66$ in the absence of inhibitory feedback ($w_{ic} = 0\,nS$) and stronger local excitation ($0.8\,nS \leq w_{ic} \leq 2\,nS$). ($C$) Increasing inhibition slowly decouples the bursts, causing the overall network synchrony to decrease to $0.48 \leq \kappa(\tau) \leq 0.59$ with $0.4\,nS \leq w_{ic} \leq 0.7\,nS$. ($D$) Stronger inhibition $0.8\,nS \leq w_{ic} \leq 2\,nS$ eliminates the bursts converting them into narrower bands of synchronous firing, increasing the network synchrony to $0.66 \leq \kappa(\tau) \leq 0.77$. ($E$) As the inhibitory to CAN connection strength w_{ic} is increased (y axis) the synchronisation of the firing activity ($\kappa(\tau)$) in the CAN population increases from $\kappa(\tau) = 0.32$ (A) to $\kappa(\tau) \geq 0.66$ (D), for several CAN-CAN connection weights $0.72\,nS \leq w_{cc} \leq 1.08\,nS$ (x

axis). When starting from a CAN pyramidal synchronous firing regime ($w_{cc} \geq 0.8\,nS$ as shown in (B)) the network synchronisation measure initially decreases as stronger inhibition desynchronises the pyramidal bursts (C). Eventually, the bursts become narrower bands of synchronous firing (C) yielding a higher network synchrony measure. Parameters are: $g_{\text{CAN}} = \mathcal{N}(22.5, 5)\,\mu S\,cm^{-2}$, $g_{\text{M}} = 45\,\mu S\,cm^{-2}$, $w_{cc} = 0.92\,nS$, $w_{ci} = 1\,nS$, $w_{ii} = 0.5\,nS$. $\kappa(\tau)$ is comprised between 0 and 1, representing an asynchronous population firing and fully synchronised firing respectively.

Fig. 5. Modulating theta oscillations frequency and power. (A) Theta oscillations power is modulated by the CAN conductance in the 100-cell CAN pyramidal network, showing a peak at $f_{osc} = 4.88\,Hz$ for $g_{\text{CAN}} = \mathcal{N}(46.5, 5)\,\mu S\,cm^{-2}$. The theta frequency range displayed by the network is $4\,Hz \leq f_{osc} \leq 7\,Hz$. (B) CAN Conductance modulates theta oscillations frequency and power in the CAN-Inh network. Increasing the CAN conductance accelerates the firing rate of the pyramidal neurons which in turn causes them to receive a surge of feedback inhibition, tightening the synchronisation and accelerating their oscillatory behaviour. The maximum theta power is at $f_{osc} = 8.54\,Hz$ for $g_{CAN} = \mathcal{N}(56.9, 5)\,\mu S\,cm^{-2}$. The theta frequency range displayed by the network is $4\,Hz \leq f_{osc} \leq 11\,Hz$. Parameters for the CAN-only network are: $\mathcal{N}(20, 5)\,\mu S\,cm^{-2} \leq g_{\text{CAN}} \leq \mathcal{N}(70, 5)\,\mu S\,cm^{-2}$, $g_{\text{M}} = 90\,\mu S\,cm^{-2}$, and $w_{cc} = 0.51\,nS$. Parameters for the CAN-Inh network are: $\mathcal{N}(20, 5)\,\mu S\,cm^{-2} \leq g_{\text{CAN}} \leq \mathcal{N}(70, 5)\,\mu S\,cm^{-2}$, $g_{\text{M}} = 90\,\mu S\,cm^{-2}$, $w_{cc} = 1.44\,nS$, $w_{ci} = 0.8\,nS$, $w_{ii} = 1.0\,nS$, and $w_{ic} = 1.4\,nS$.

Figures

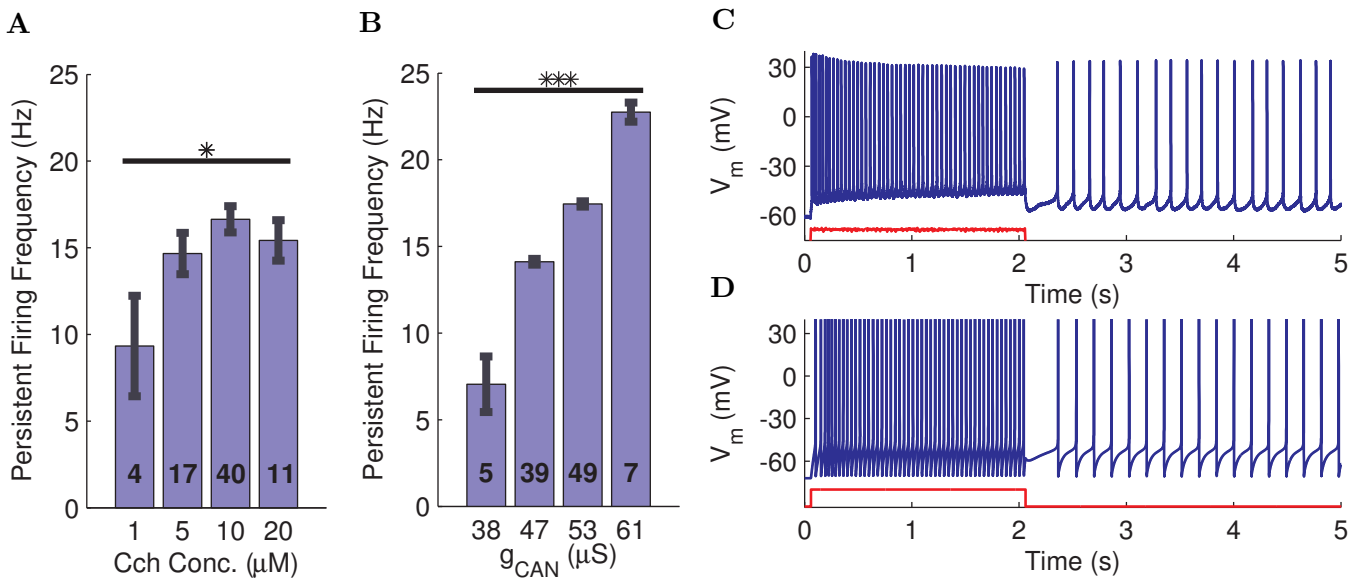

Fig. 1. The activation of CAN receptors modulates the persistent firing frequency of hippocampal neurons, both *in vitro* and in the model. (A) The carbachol concentration (μM) modulates the persistent firing frequency recorded *in vitro*. (B) Similary, the CAN conductance (g_{CAN}) modulates the persistent firing frequency of the simulated neurons. Line and asterisks over bars indicate statistical significance. Numbers inside the bars represent the cell count. (C) Sample *in-vitro* recording of the membrane potential (V_m) of one CA1 pyramidal neuron showing approximately $6\,Hz$ persistent firing after a $2\,s$ stimulation. (D) Sample voltage trace for one simulated neuron showing approximately $6\,Hz$ persistent firing after a $2\,s$ stimulation. In the voltage trace plots the bottom line represents the applied square pulse stimulation current. Persistent firing is elicited after a brief $(2\,s)$ stimulation. Parameters for the CAN pyramidal neurons shown in the histogram are: $g_{\text{CAN}} = \mathcal{N}(50, 5)\,\mu S\,cm^{-2}$, $g_{\text{M}} = 90\,\mu S\,cm^{-2}$.

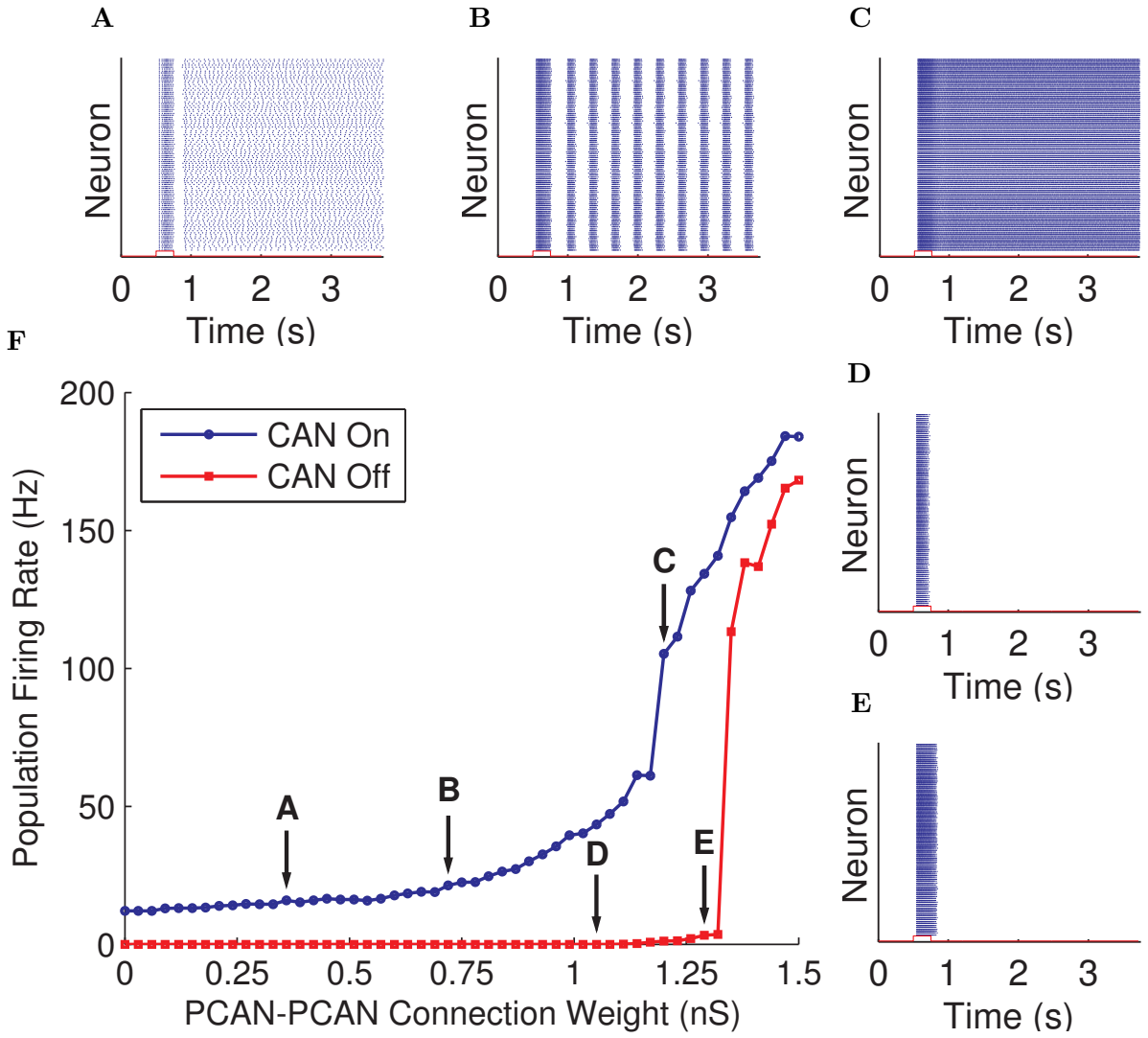

Fig. 2. The CAN current activation allows a 100-cell network to display persistent firing in biologically plausible frequency bands. (A) CAN-enabled Network – Sample raster plot of the slow regime ($0\,nS \leq w_{cc} \leq 0.45\,nS$), with a population firing rate of $f = 19.45\,Hz$ for $w_{cc} = 0.36\,nS$. (B) CAN-enabled Network – Sample raster plot of the synchronous bursting firing regime ($0.48\,nS \leq w_{cc} \leq 1.17\,nS$), showing $f_{osc} = 5\,Hz$ oscillations for $w_{cc} = 0.72\,nS$. (C) CAN-enabled Network – Sample raster plot of the fast firing regime ($w_{cc} \geq 1.2\,nS$), with a population firing rate $f = 117.3\,Hz$ for $w_{cc} = 1.2\,nS$. (D) CAN-disabled Network – Sample raster plot showing the lack of persistent firing in the absence of CAN current ($0\,nS \leq w_{cc} \leq 1.08\,nS$). (E) CAN-disabled Network – Sample raster plot showing firing activity persisting for a few milliseconds after the stimulation is removed ($1.11\,nS \leq w_{cc} \leq 1.32\,nS$), with a population firing rate $0.08\,Hz \leq f \leq 3.56\,Hz$. (F) The population firing frequencies of the CAN pyramidal network span $14\,Hz \leq f \leq 120\,Hz$, with $0\,nS \leq w_{cc} \leq 1.23\,nS$. The CAN network (top line) displays three different firing regimes: a slow regime with firing rates $14\,Hz \leq f \leq 21\,Hz$ (A), a synchronous bursting regime (B), and a fast spiking regime with firing rates $f \geq 117\,Hz$ (C). Conversely, a pyramidal network without CAN current (bottom line) does not display such a rich array of firing regimes (D and E). Parameters are: $g_{\mathrm{CAN}} = \mathcal{N}(50, 5)\,\mu S\,cm^{-2}$, $g_{\mathrm{M}} = 90\,\mu S\,cm^{-2}$, $0 \leq w_{cc} \leq 1.5\,nS$.

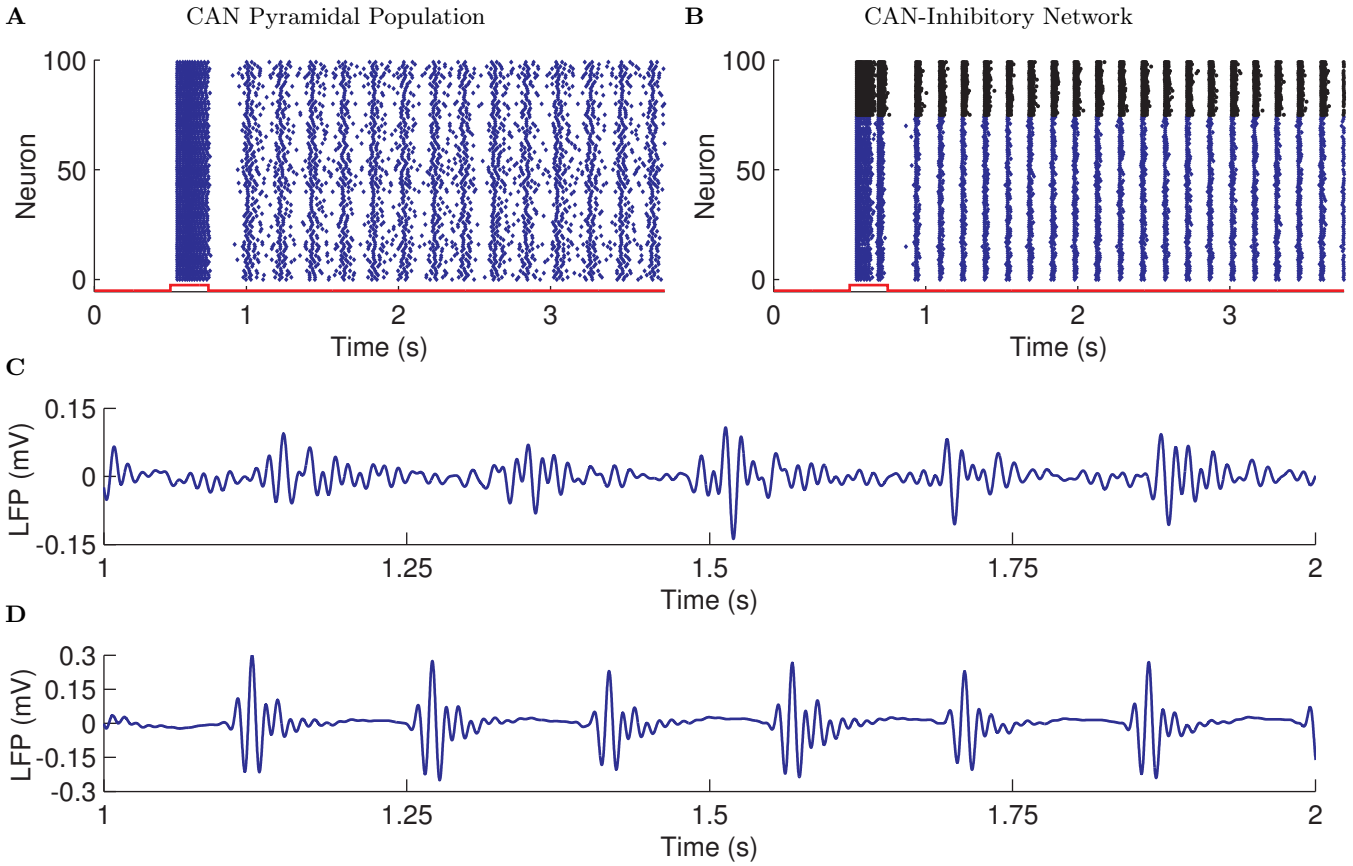

Fig. 3. Comparison of CAN and CAN-In network dynamics. (A) Raster plot for the 100-cell CAN pyramidal network, showing 5.46 Hz oscillations with a synchronisation of $\kappa(\tau) = 0.38$, $\tau = 10\,ms$. (B) Raster plot for the CAN-Inhibitory network comprising 75 CAN pyramidal cells (cell number $0 - 74$, blue diamonds) and 25 inhibitory cells (cell number $75 - 99$, black dots), showing 6.91 Hz oscillations with a synchronisation of $\kappa(\tau) = 0.78$, $\tau = 10\,ms$. In both plots the red line below the raster represents the applied stimulation current. (C) LFP signal computed from the spiking activity of the CAN pyramidal network shows nested gamma in theta oscillations (one-second extract). (D) LFP signal computed from the spiking activity of the CAN-Inhibitory network shows nested gamma in theta oscillations with higher amplitudes compared to the CAN pyramidal network (one-second extract). Parameters for the CAN-only network are: $g_{\mathrm{CAN}} = \mathcal{N}(50, 5)\,\mu S\,cm^{-2}$, $g_{\mathrm{M}} = 90\,\mu S\,cm^{-2}$, $w_{cc} = 0.48\,nS$. Parameters for the CAN-Inhibitory network are: $g_{\mathrm{CAN}} = \mathcal{N}(50, 5)\,\mu S\,cm^{-2}$, $g_{\mathrm{M}} = 90\,\mu S\,cm^{-2}$, $w_{cc} = 1.44\,nS$, $w_{ci} = 1\,nS$, $w_{ii} = 1.0\,nS$, $w_{ic} = 1.2\,nS$.

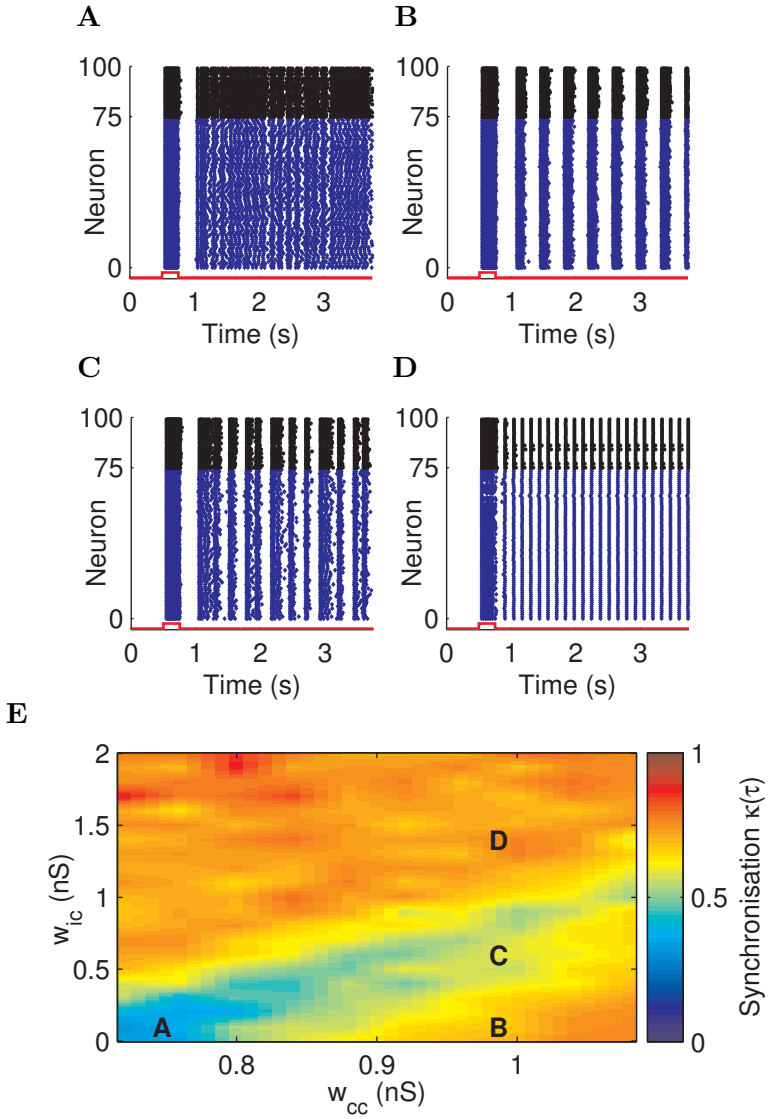

Fig. 4. Feedback inhibition synchronises CAN-mediated persistent activity. (A) Sample raster plot of the asynchronous firing regime showing a synchrony measure of $\kappa(\tau) = 0.32$ in the absence of inhibitory feedback ($w_{ic} = 0\,nS$) and weaker local excitation ($w_{cc} < 0.8\,nS$). (B) Sample raster plot of the synchronous bursting firing regime showing a synchrony measure of $\kappa(\tau) = 0.66$ in the absence of inhibitory feedback ($w_{ic} = 0\,nS$) and stronger local excitation ($0.8\,nS \leq w_{ic} \leq 2\,nS$). (C) Increasing inhibition slowly decouples the bursts, causing the overall network synchrony to decrease to $0.48 \leq \kappa(\tau) \leq 0.59$ with $0.4\,nS \leq w_{ic} \leq 0.7\,nS$. (D) Stronger inhibition $0.8\,nS \leq w_{ic} \leq 2\,nS$ eliminates the bursts converting them into narrower bands of synchronous firing, increasing the network synchrony to $0.66 \leq \kappa(\tau) \leq 0.77$. (E) As the inhibitory to CAN connection strength w_{ic} is increased (y axis) the synchronisation of the firing activity ($\kappa(\tau)$) in the CAN population increases from $\kappa(\tau) = 0.32$ (A) to $\kappa(\tau) \geq 0.66$ (D), for several CAN-CAN connection weights $0.72\,nS \leq w_{cc} \leq 1.08\,nS$ (x axis). When starting from a CAN pyramidal synchronous firing regime ($w_{cc} \geq 0.8\,nS$ as shown in (B)) the network synchronisation measure initially decreases as stronger inhibition desynchronises the pyramidal bursts (C). Eventually, the bursts become narrower bands of synchronous firing (C) yielding a higher network synchrony measure. Parameters are: $g_{\text{CAN}} = \mathcal{N}(22.5, 5)\,\mu S\,cm^{-2}$, $g_{\text{M}} = 45\,\mu S\,cm^{-2}$, $w_{cc} = 0.92\,nS$, $w_{ci} = 1\,nS$, $w_{ii} = 0.5\,nS$. $\kappa(\tau)$ is comprised between 0 and 1, representing an asynchronous population firing and fully synchronised firing respectively.

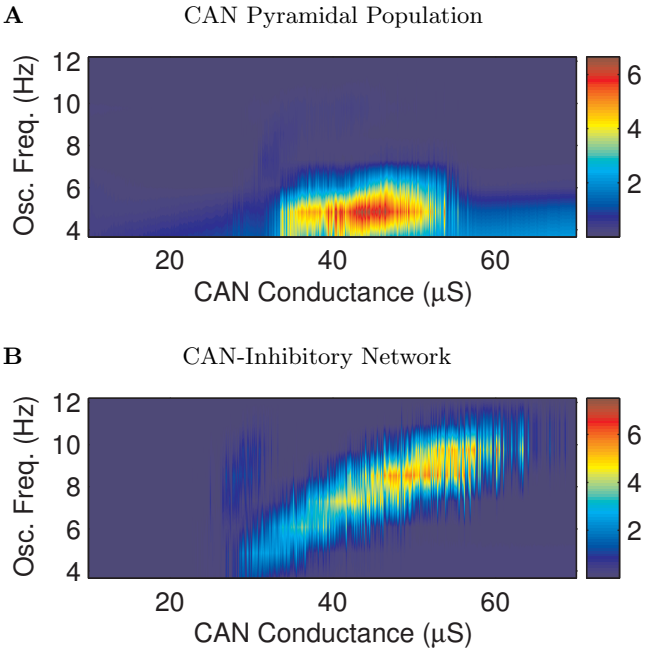

Fig. 5. Modulating theta oscillations frequency and power. (A) Theta oscillations power is modulated by the CAN conductance in the 100-cell CAN pyramidal network, showing a peak at $f_{osc} = 4.88\,Hz$ for $g_{\mathrm{CAN}} = \mathcal{N}(46.5, 5)\,\mu S\,cm^{-2}$. The theta frequency range displayed by the network is $4\,Hz \leq f_{osc} \leq 7\,Hz$. (B) CAN Conductance modulates theta oscillations frequency and power in the CAN-Inh network. Increasing the CAN conductance accelerates the firing rate of the pyramidal neurons which in turn causes them to receive a surge of feedback inhibition, tightening the synchronisation and accelerating their oscillatory behaviour. The maximum theta power is at $f_{osc} = 8.54\,Hz$ for $g_{CAN} = \mathcal{N}(56.9, 5)\,\mu S\,cm^{-2}$. The theta frequency range displayed by the network is $4\,Hz \leq f_{osc} \leq 11\,Hz$. Parameters for the CAN-only network are: $\mathcal{N}(20, 5)\,\mu S\,cm^{-2} \leq g_{\mathrm{CAN}} \leq \mathcal{N}(70, 5)\,\mu S\,cm^{-2}$, $g_{\mathrm{M}} = 90\,\mu S\,cm^{-2}$, and $w_{cc} = 0.51\,nS$. Parameters for the CAN-Inh network are: $\mathcal{N}(20, 5)\,\mu S\,cm^{-2} \leq g_{\mathrm{CAN}} \leq \mathcal{N}(70, 5)\,\mu S\,cm^{-2}$, $g_{\mathrm{M}} = 90\,\mu S\,cm^{-2}$, $w_{cc} = 1.44\,nS$, $w_{ci} = 0.8\,nS$, $w_{ii} = 1.0\,nS$, and $w_{ic} = 1.4\,nS$.